

Scattering anisotropy in HgTe (013) quantum well

D. A. Khudaiberdiev,^{1,2} M. L. Savchenko,^{1,3} D. A. Kozlov,^{1,2} N. N. Mikhailov,^{1,2} and Z. D. Kvon^{1,2}

¹⁾*Rzhanov Institute of Semiconductor Physics, Novosibirsk 630090, Russia*

²⁾*Novosibirsk State University, Novosibirsk 630090, Russia*

³⁾*Institute of Solid State Physics, Vienna University of Technology, 1040 Vienna, Austria*

(*Electronic mail: KhudaiberdievDA@gmail.com)

(Dated: 2 June 2022)

We report on a detailed experimental study of the electron transport anisotropy in HgTe (013) quantum well of 22 nm width in the directions [100] and $[03\bar{1}]$ as the function of the electron density n . The anisotropy is absent at minimal electron density near the charge neutrality point. The anisotropy increases with the increase of n and reaches about 10% when the Fermi level is within the first subband H1. There is a sharp increase of the anisotropy (up to 60%) when the Fermi level reaches the second subband E2. We conclude that the first effect is due to the small intra-subband anisotropic interface roughness scattering, and the second one is due to the strongly anisotropic inter-subband roughness scattering, but the microscopical reason of such a strong change in the anisotropy remains unknown.

Experimental studies of HgTe-based quantum wells (QW) are among the most actively developing directions of research in the physics of low-dimensional electron systems. Due to the strong relativistic effects in these QWs, different kinds of two-dimensional (2D) systems can be realized from them. Films with thickness lower than critical (6.5 nm) are ordinary 2D insulators when the Fermi energy lies inside the band gap. When the thickness is higher than critical, the hole-like subband H1 lies above the electron-like subband E1, so the system becomes two-dimensional topological insulator¹⁻⁴. At critical thickness Dirac fermion system occurs⁵⁻⁸. At higher thicknesses (starting with 14 nm) H2 and H1 subbands overlap creating 2D semimetal state⁹⁻¹³.

The most qualitative HgTe QWs are grown by molecular beam epitaxy in nonsingular directions such as (013) and (112) with electron mobility reaching the values of about $10^6 \text{ cm}^2/\text{Vs}$. The reason of using such directions is to increase the dissociation rate of Te_2 molecules (so to prevent crystallisation of clean Te) that is preferred near surface steps¹⁴. In different 2D electron systems (based on GaAs/AlAs inverted interface¹⁵, InAs¹⁶, InSb¹⁷ and Ge¹⁸ QWs) anisotropic transport caused by anisotropic scattering on surface roughness had been studied. In those works, even with (001) direction of growth, scattering on roughness has preferred direction [110] which leads to the mobility anisotropy. Thus, HgTe QWs with (013) nonsingular direction of growth are even more expected to have scattering anisotropy. We note that such anisotropy in HgTe (013) QW was observed before¹¹ but there non-inverted 5 nm-thick low electron mobility system was studied.

In this paper we study electron transport anisotropy in 22-nm HgTe QWs with inverted spectrum, so that the first two conduction subbands are H1 and E2. We report a transport anisotropy caused by anisotropic roughness scattering when the Fermi level crosses only H1 subband, and a non-trivial jump of anisotropy when the Fermi level reaches the second subband E2 caused by strongly anisotropic intra-subband scattering.

The studied QWs are realised on the HgTe/Hg_{0.35}Cd_{0.65}Te heterostructure grown by molecular beam epitaxy on a GaAs (013) substrate (Fig. 1 (a)). The system is equipped with Ti/Au metallic gate which is located above 100 nm +

200 nm $\text{SiO}_2/\text{Si}_3\text{N}_4$ insulator layers. Several L -shaped Hall

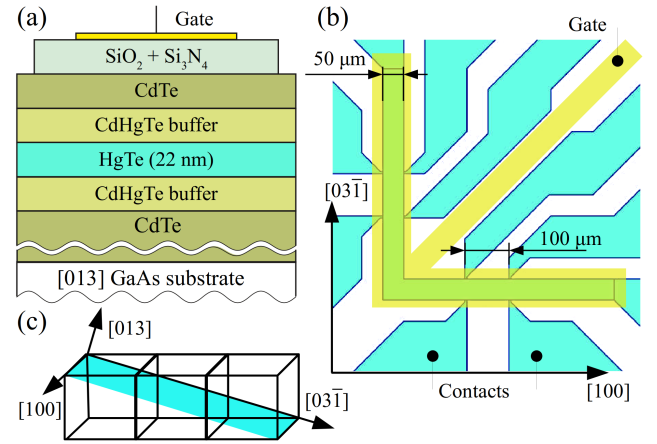


FIG. 1. (a) Schematic cross section of the heterostructures studied. The HgTe 22 nm film is located between $\text{Cd}_{0.65}\text{Hg}_{0.35}\text{Te}$ buffer layers. (b) Schematic top view of the L -shaped mesa structure with $[100]$ and $[03\bar{1}]$ arms orientations. (c) Crystallographic directions in the system.

bar devices are prepared, they gave quantitatively similar results, thus we present data from one device. The L -shaped arm orientations are symmetric $[100]$ and non-symmetric $[03\bar{1}]$ (Fig. 1 (b)). The symmetry-based names are illustrated in panel (c), where studied crystallographic directions are schematically presented. The current channel width is 50 μm , the distance between pairs of longitudinal potential probes is 100 μm . All the measurements were carried out using a standard lock-in technique with about 12 Hz frequency and $(0.01 - 1) \mu\text{A}$ applied current in a perpendicular magnetic field B up to 1.5 T. All presented results were obtained at temperature 0.2 K.

Fig. 2 (a) demonstrates the main result of our work – the gate voltage dependencies of the longitudinal resistance in directions $[100]$ and $[03\bar{1}]$. Qualitatively one can see the ordinary for (18-22) nm HgTe QWs gate voltage dependencies of resistance in both orientations: they have a maximum near the

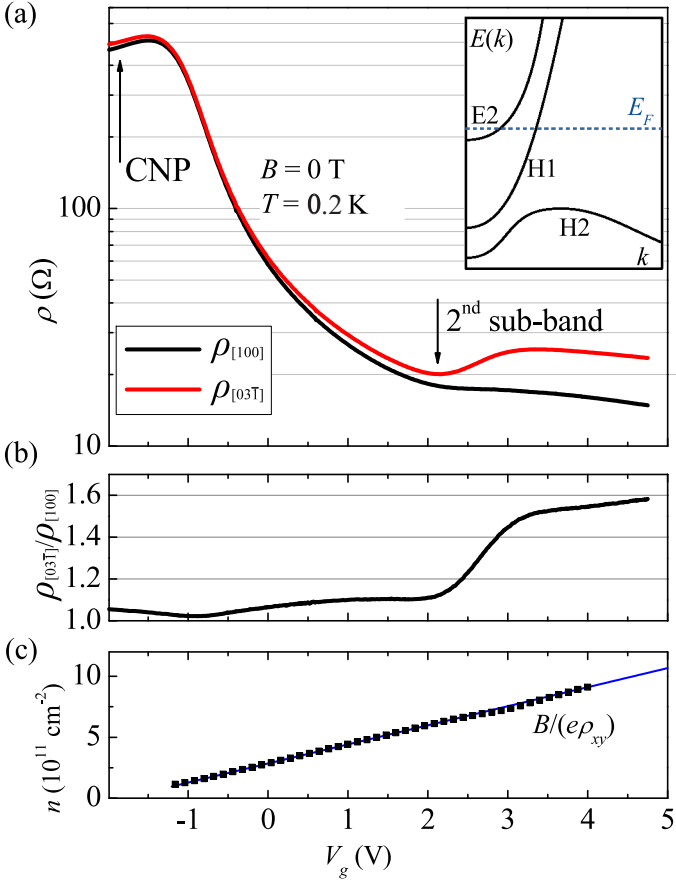


FIG. 2. (a) The gate voltage dependence of the longitudinal resistance in different directions: [100] (black) and [03T] (red). (b) The gate voltage dependence of the resistance anisotropy $\rho_{[03T]}/\rho_{[100]}$. (c) The gate voltage dependence of the electron density (symbols) that was determined from the Hall effect measurements at $B = 0.5$ T.

charge neutrality point (CNP), and there is a sharp decrease of resistances as the gate voltage increases. In the vicinity of CNP the resistance behaviour is slightly anisotropic (see the gate voltage dependence of the resistance anisotropy ratio $\rho_{[03T]}/\rho_{[100]}$ in Fig. 2(b)) due to the hole mass anisotropy^{19,20} (the presence of holes is seen in Fig. 3 as a sign-alternating $\rho_{xy}(B)$ dependence measured at $V_g = -2.5$ V (violet symbols)), we do not discuss this region in current paper. There are no holes already at $V_g = -1$ V (see linear $\rho_{xy}(B)$ in Fig. 3, green symbols), and the transport is fully isotropic here. At higher gate voltages the difference between $\rho_{[03T]}$ and $\rho_{[100]}$ gradually increases and their ratio saturates at around $\rho_{[03T]}/\rho_{[100]} \approx 1.1$. Surprisingly, at $V_g = 2$ V the resistance along the direction [03T] starts to increase, while $\rho_{[100]}$ continues to decrease, so their ratio $\rho_{[03T]}/\rho_{[100]}$ jumps from 1.1 to 1.5 value. And there is again only a moderate increase of the anisotropy ratio at higher gate voltages.

Such unexpected behaviour with the sharp increase of the anisotropy ratio at $V_g \approx (2 - 3)$ V should come from a new scattering mechanism that start in this gate voltage range, and that has a strong orientation dependence. But before dis-

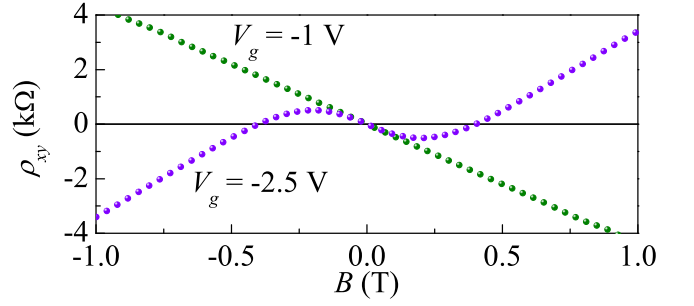


FIG. 3. $\rho_{xy}(B)$ at $V_g = -1$ V (olive) and $V_g = -2.5$ (violet). The nonlinear Hall resistance measured at -2.5 V suggests the existence of holes and electrons at this V_g .

cussing the origin of the such anisotropy dependence let's analyze other transport properties of the system.

In Fig. 4(a) we show examples of normalized Shubnikov – de Haas (SdH) resistance oscillations $\Delta\rho_{xx}/\rho_{xx}^0$ measured at different gate voltages vs a reciprocal magnetic field B^{-1} . Corresponding fast Fourier transform (FFT) spectra are shown in panel (b). Several peaks at frequencies f_i occur on each spectra. It is seen that at $V_g < 3$ V there is only one peak f_1 or there are two close to each other peaks $f_{1,2}$ that arise on the place of peak f_1 at higher densities. At $V_g > 3$ V there is also one more low-frequency (e.g., low-density) peak f_3 . These frequencies are translated to the density values according to the standard relation $n_i^{\text{SdH}} = g_i(e/h)f_i$ (where g_i is a spin degeneracy, e is the elementary charge, h is the Planck constant), and depicted in Fig. 4(c) as empty symbols. It is logical to assume that f_1 and f_2 peaks come from spin-resolved Landau levels, so they have $g_{1,2} = 1$, and they originate from the first conduction subband H1 (see the inset of Fig. 2(a)). The low-frequency f_3 peak is attributed to the spin-degenerate electrons from the second conduction subband E2. In Fig. 4(c) we also plot the total SdH density $n_{\Sigma}^{\text{SdH}} = n_1^{\text{SdH}} + n_2^{\text{SdH}} + n_3^{\text{SdH}}$ (red filled squares) and the density obtained from the Hall measurements (blue line from Fig. 2(c)) that coincide quite well that approves suggested carrier identification. Furthermore, electrons from the second conduction subband were recently detected at similar total density in the cyclotron resonance measurements in Ref. 20, where the same 22-nm HgTe QW was studied. The coincidence of the gate voltages $V_g \approx (2 - 3)$ V at which the resistance anisotropy $\rho_{[03T]}/\rho_{[100]}$ sharply increases (Fig. 2(b)), and at which electrons start to occupy the E2 subband allows as to connect these two effects.

Now let's discuss the origin of the resistance anisotropy. In fact, there are two types of behaviour on $\rho_{[03T]}/\rho_{[100]}(V_g)$ dependence in Fig. 2(b). First, there is a slow trend of the increase of the anisotropy with the increase of the electron density. Second, there is a sharp anisotropy increase around 2.5 V as the Fermi level touches the second subband E2. Since the anisotropy of the electron energy in the conduction bands of HgTe (013) quantum wells is rather weak, the observed resistance anisotropy has to be induced by the scattering anisotropy. At low temperatures, when the phonon scattering is frozen, the main sources of scattering are impurities

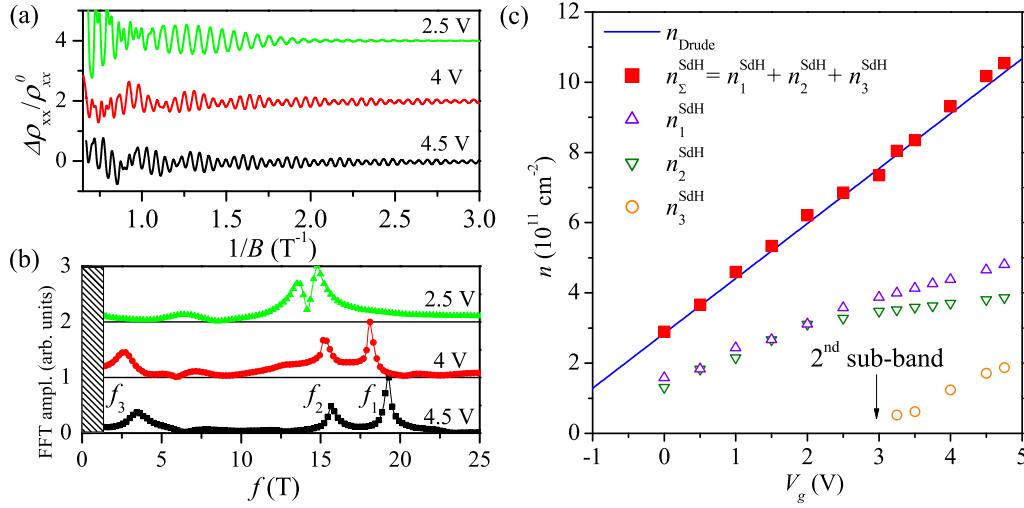


FIG. 4. (a) The normalized resistance oscillations $\Delta\rho_{xx}/\rho_{xx}^0 = (\rho_{xx} - \langle\rho_{xx}\rangle)/\rho_{xx}^0$ on the B^{-1} scale, where $\langle\rho_{xx}\rangle$ is the monotonous part of ρ_{xx} and ρ_{xx}^0 is $\rho_{xx}(B=0)$. (b) The Fourier spectra of the SdH oscillations. (c) The gate voltage density dependencies for concentrations obtained from classical measurements (n_{Drude}) and SdH oscillation analysis (n^{SdH}). Olive and violet triangles refer to spin-split electrons from subband H1, while orange circles – to electrons from the second subband E2. The sum of all concentrations received from SdH analysis n_{Σ}^{SdH} (red squares) fits n_{Drude} .

and roughness of the quantum well interfaces.

Here we suggest a simple model to explain the observed anisotropy behaviour. Let's assume that only electrons from the first subband H1 contribute to the transport (having higher density and mobility), while E2 electrons participate only in screening and, most importantly, in the inter-subband scattering of H1 electrons. Thus, we consider the following three mechanisms of scattering: impurities scattering, intra-subband roughness scattering, and inter-subband roughness scattering. And only last two are considered to be anisotropic. For a longitudinal term of the inverted mobility tensor depending on the in-plane angle θ from the direction [001] we write

$$\frac{1}{\mu} = \frac{1}{\mu_{imp}} + \frac{1 + A_r \sin^2 \theta}{\mu_r} + \frac{1 + A_{ISB} \sin^2 \theta}{\mu_{ISB}}, \quad (1)$$

where μ_{imp} , μ_r and μ_{ISB} are isotropic contributions of impurities, roughness and inter-subband scatterings, respectively. Here we introduce two phenomenological parameters A_r and A_{ISB} that determine anisotropy of roughness and inter-subband scattering rates. The two steps fitting was performed to determine these parameters (Fig. 5). By fitting $\mu(n)$ in the [001] direction with only isotropic contributions we derived the impurity scattering parameters: the number of impurities, height and correlation length of roughness, and the intensity of inter-subband scattering (here we used a model developed in Ref. 21). Then, by fitting $\mu(n)$ in the direction [03 $\bar{1}$] we derived $A_r \approx 0.2$ and $A_{ISB} \approx 1$. As usual, impurity scattering dominates at lower electron density, and roughness scattering dominates at higher density. So at lower densities the anisotropy ratio is closer to unity because the isotropic scattering mechanism – the impurity scattering – dominates. And at higher densities (but still at $V_g < 2V$) the resistance anisotropy increases to 1.1 because of the increase of the impact of the

roughness scattering anisotropy with $A_r \approx 0.2$. And finally, at even higher density, when E2 subband states appear, the anisotropic inter-subband scattering with $A_{ISB} \approx 1$ starts to dramatically increase the anisotropy ratio.

We need to note that it is worth nothing to make a microscopical model that will explain the measured anisotropy in the only first subband by non-symmetrical form of roughness¹⁵. The problem here is to explain the anisotropy of both inter- and intra-subband scattering together withing such a model. We tried to perform such a microscopical calculations with different forms of roughness, but neither elliptical, nor even one-dimensional roughness give such strong anisotropic inter-subband scattering with simultaneously small anisotropy in the intra-subband scattering. The only successful attempt to fit the experiment was to consider that one component of the H1 subband wave function near the interface strongly depends on the in-plane angle, and that only this component scatters to E2 subband states. Nevertheless, the kp calculations do not support this assumption, so the microscopic origin of the strong inter-subband anisotropy in HgTe (013) system remains open as a challenge for the theory.

ACKNOWLEDGMENTS

We thank E. G. Novik, S. A. Tarasenko and M. V. Entin for helpful discussions.

DATA AVAILABILITY STATEMENT

The data that support the findings of this study are available from the corresponding author upon reasonable request.

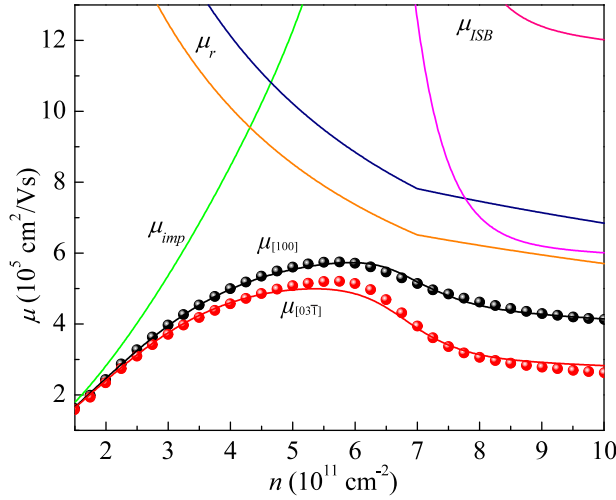


FIG. 5. Experimental (circles) and theoretical (lines) mobility of electrons in both directions depending on a electron concentration n . Green line refers to impurity scattering contribution, blue and orange lines — to intra-subband roughness scattering contribution, violet and purple lines — to inter-subband roughness scattering contribution for both directions.

- ¹M. König, S. Wiedmann, C. Brüne, A. Roth, H. Buhmann, L. W. Molenkamp, X.-L. Qi, and S.-C. Zhang, “Quantum spin hall insulator state in hgte quantum wells,” *Science* **318**, 766–770 (2007).
- ²K. C. Nowack, E. M. Spanton, M. Baenninger, M. König, J. R. Kirtley, B. Kalisky, C. Ames, P. Leubner, C. Brüne, H. Buhmann, L. W. Molenkamp, D. Goldhaber-Gordon, and K. A. Moler, “Imaging currents in HgTe quantum wells in the quantum spin Hall regime,” *Nature Materials* **12**, 787–791 (2013).
- ³M. König, M. Baenninger, A. G. Garcia, N. Harjee, B. L. Pruitt, C. Ames, P. Leubner, C. Brüne, H. Buhmann, L. W. Molenkamp, and D. Goldhaber-Gordon, “Spatially resolved study of backscattering in the quantum spin Hall state,” *Physical Review X* **3**, 1–9 (2013), arXiv:1211.3917.
- ⁴K. M. Dantscher, D. A. Kozlov, M. T. Scherr, S. Gebert, J. Bärenfänger, M. V. Durnev, S. A. Tarasenko, V. V. Bel’Kov, N. N. Mikhailov, S. A. Dvoretzky, Z. D. Kvon, J. Ziegler, D. Weiss, and S. D. Ganichev, “Photogalvanic probing of helical edge channels in two-dimensional HgTe topological insulators,” *Physical Review B* **95**, 3–7 (2017).
- ⁵B. Büttner, C. X. Liu, G. Tkachov, E. G. Novik, C. Brüne, H. Buhmann, E. M. Hankiewicz, P. Recher, B. Trauzettel, S. C. Zhang, and L. W. Molenkamp, “Single valley Dirac fermions in zero-gap HgTe quantum wells,” *Nature Physics* **7**, 418–422 (2011), arXiv:1009.2248.

- ⁶Z. D. Kvon, S. N. Danilov, D. A. Kozlov, C. Zoth, N. N. Mikhailov, S. A. Dvoretzky, and S. D. Ganichev, “Cyclotron Resonance of Dirac Fermions in HgTe Quantum Wells,” *JETP Lett.* **94**, 816–819 (2011).
- ⁷D. A. Kozlov, Z. D. Kvon, N. N. Mikhailov, and S. A. Dvoretzky, “Weak localization of Dirac fermions in HgTe quantum wells,” *JETP Lett.* **96**, 815 (2012).
- ⁸G. M. Gusev, D. A. Kozlov, A. D. Levin, Z. D. Kvon, N. N. Mikhailov, and S. A. Dvoretzky, “Robust helical edge transport at $\nu=0$ quantum Hall state,” *Physical Review B* **96**, 1–5 (2017).
- ⁹Z. D. Kvon, E. B. Olshanetsky, D. A. Kozlov, N. N. Mikhailov, and S. A. Dvoretzky, “Two-dimensional electron-hole system in a HgTe-based quantum well,” *JETP Lett.* **87**, 502–505 (2008).
- ¹⁰E. B. Olshanetsky, Z. D. Kvon, M. V. Entin, L. I. Magarill, N. N. Mikhailov, I. O. Parm, and S. A. Dvoretzky, “Scattering processes in a two-dimensional semimetal,” *JETP Lett.* **89**, 290–293 (2009).
- ¹¹G. M. Minkov, A. V. Germanenko, O. E. Rut, A. A. Sherstobitov, S. A. Dvoretzky, and N. N. Mikhailov, “Anisotropic conductivity and weak localization in HgTe quantum wells with a normal energy spectrum,” *Physical Review B* **88**, 045323 (2013).
- ¹²M. Knap, J. D. Sau, B. I. Halperin, and E. Demler, “Transport in two-dimensional disordered semimetals,” *Physical Review Letters* **113**, 1–5 (2014), arXiv:1405.0277.
- ¹³A. Kononov, S. V. Egorov, Z. D. Kvon, N. N. Mikhailov, S. A. Dvoretzky, and E. V. Deviatov, “Andreev reflection at the edge of a two-dimensional semimetal,” *Physical Review B* **93**, 1–5 (2016), arXiv:1511.08085.
- ¹⁴Z. D. Kvon, E. B. Olshanetsky, N. N. Mikhailov, and D. A. Kozlov, “Two-dimensional electron systems in HgTe quantum wells,” *Low Temperature Physics* **35**, 6–14 (2009).
- ¹⁵Y. Markus, U. Meirav, H. Shtrikman, and B. Laikhtman, “Anisotropic mobility and roughness scattering in a 2D electron gas,” *Semiconductor Science and Technology* **9**, 1297–1304 (1994).
- ¹⁶S. P. Le and T. K. Suzuki, “Electron mobility anisotropy in InAs/GaAs(001) heterostructures,” *Applied Physics Letters* **118**, 1–6 (2021).
- ¹⁷M. A. Ball, J. C. Keay, S. J. Chung, M. B. Santos, and M. B. Johnson, “Mobility anisotropy in InSb/AlxIn1-xSb single quantum wells,” *Applied Physics Letters* **80**, 2138–2140 (2002).
- ¹⁸A. H. Hassan, R. J. Morris, O. A. Mironov, R. Beanland, D. Walker, S. Huband, A. Dobbie, M. Myronov, and D. R. Leadley, “Anisotropy in the hole mobility measured along the [110] and [1-10] orientations in a strained Ge quantum well,” *Applied Physics Letters* **104** (2014), 10.1063/1.4870392.
- ¹⁹G. M. Minkov, V. Y. Aleshkin, O. E. Rut, A. A. Sherstobitov, A. V. Germanenko, S. A. Dvoretzky, and N. N. Mikhailov, “Valence band energy spectrum of HgTe quantum wells with an inverted band structure,” *Physical Review B* **96**, 1–8 (2017), arXiv:1705.04717.
- ²⁰J. Gospodarič, A. Shuvaev, N. N. Mikhailov, Z. D. Kvon, E. G. Novik, and A. Pimenov, “Energy spectrum of semimetallic HgTe quantum wells,” *Physical Review B* **104**, 1–7 (2021), arXiv:2109.07254.
- ²¹A. A. Dobretsova, L. S. Braginskii, M. V. Entin, Z. D. Kvon, N. N. Mikhailov, and S. A. Dvoretzky, “Surface states in a HgTe quantum well and scattering by surface roughness,” *JETP Lett.* **101**, 330 (2015).